Effect of actual and accelerated ageing on microstructure evolution and mechanical properties of a 2024-T351 aluminium alloy

M. Prudhomme, F. Billy, Joel Alexis, G. Benoit, F. Hamon, C. Larignon, G. Odemer, C. Blanc, Gilbert Hénaff

Effect of actual and accelerated ageing on microstructure evolution and mechanical properties of a 2024-T351 aluminium alloy

M. Prudhomme[a,b], F. Billy[a], J. Alexis[c], G. Benoit[a], F. Hamon[a], C. Larignon[b], G. Odemer[b], C. Blanc[b] and G. Hénaff[a, *]

[a] Pprime Institute, UPR 3346 CNRS-ENSMA-Université de Poitiers, ISAE-ENSMA, 1 avenue Clément Ader, 86961 Futuroscope Chasseneuil, France

[b] CIRIMAT, Université de Toulouse, CNRS, INPT, UPS, ENSIACET, 4, allée Emile Monso BP 44362, 31030 Toulouse Cedex 4, France

[c] LGP, ENIT, 47 avenue d'Azereix - BP 1629 - 65016 Tarbes CEDEX, France

Abstract

Due to the increasing number of civil transport aircrafts that come close to the end of the initial design life, airliners as well as aircraft manufacturers have to face different challenges. Indeed, in addition to the life extension concerns, the development of an enhanced knowledge of the structural health during life is a key issue in order to manage the fleet in service, but also to improve the design of new aircrafts. With this respect, the French National program DIAGNOSTAT, sponsored by an Inter-ministerial Fund and endorsed by Aerospace Valley competitiveness cluster, was undertaken with the global objective of getting a feedback on the aircraft structural health at the end of the initial design life and of developing innovative non-destructive techniques to monitor this structural health. The study presented here is more particularly concerned with the first point, and with the ageing effect on the properties of the 2024-T351 aluminium alloy.

1. Introduction

This paper presents an investigation on the effects of ageing on the microstructure and the corresponding physical and mechanical properties of a 2024 aluminium alloy used in a civil transport aircraft wing structure in order to assess the residual resistance of the end of a service life. More precisely, heat treatments are applied in order to simulate thermal ageing actually endured by the structure during service. The results of characterisation of microstructural, physical and mechanical properties are compared not only to the data obtained on a pristine alloy, but also to the results obtained on coupons of a similar alloy coming from the teardown of an A320 aircraft using the same experimental procedure. The main findings are that, during a service life, no significant modification in fatigue resistance is noticed despite of changes in the precipitation structure.

The first objective of this study was to compare the residual mechanical properties of an alloy coming from the teardown of wing panels of a decommissioned AIRBUS A320 aircraft with those of a pristine alloy in relation with modifications in microstructure and physical properties. Indeed, as the metastable material constitutive of the aircraft wings have to withstand complex load and/or temperature history (that are generally ill-known), ageing effects on mechanical properties like tensile [1] and fatigue resistance [2-4] cannot be excluded. However the knowledge of the residual performances when approaching the end of the service life, and in particular of the fatigue resistance, is still extremely limited [5-7]. For instance, using a positron annihilation spectroscopy approach, Nicht et al [8] found no

[*] *Corresponding author:* gilbert.henaff@isae-ensma.fr

difference between a virgin 2024 alloy and a similar material coming from a A300 aircraft after 18 years of service. In addition the scarce results available in open literature especially about fatigue properties are somehow contradicting. Indeed, while Scheuring and Grandt [6] and Everett [5], considering the fatigue resistance of 2XXX and 7XXX alloys coming from structural parts of various retired or active aircrafts in the US, noticed no substantial difference with handbook data, Basov et al [9] report a significant decrease in fatigue strength in similar alloys coming from Russian aircrafts. The prime novelty of the work presented in this paper is therefore twofold. The first one is to compare data collected on a material that has experienced many years of real operating conditions with those obtained on a similar alloy artificially aged in laboratory conditions while the second one is to cross the results of mechanical testing with those of different techniques tracking the microstructural evolution induced by ageing. A secondary objective of the study is therefore to assess the actual degree of ageing of the material from teardown. With this aim, artificial ageing treatments have been applied on a pristine material. The relation between microstructure and mechanical properties has then been investigated at different ageing conditions using the same methodology, based on a characterisation of microstructural modification by SEM and TEM examination and conductivity measurements on the one hand and on the assessment of the impact of ageing on the mechanical properties by mechanical testing (hardness, tensile and fatigue tests) on the other hand. The data collected on artificially aged material are then compared to the information obtained on the material issued from teardown.

2. Experimental techniques and methods

2.1 Material

The pristine material used as a reference in this study was a 2024 T351 aluminium alloy provided in the form of a 50 mm rolled sheet. The final microstructure of the alloy was composed of grains elongated along the rolling direction (L) with an average grain dimension of 700 µm in the longitudinal direction. More details and fatigue data about this material are given in [10]. To evaluate the ageing stage of the 2024 alloy coming from the wing panels, artificial ageing treatments were performed on samples from the pristine material (Table 1). Artificial ageing treatments corresponded to heat treatments carried out at 150 °C for durations comprised between 0 and 177h. The durations of the treatment were actually calculated on the basic assumption that ageing is controlled by the diffusion of copper atoms, and by considering an equivalence rule between the duration and the temperature of the heat treatment [11]. The aim was to reproduce exposure of an aircraft at a mean temperature of 80 °C for a maximum duration of 319 676 h, i.e. more than 30 years. Typically, using this rule, a 100 000h exposure at 80 °C corresponded to the service life of an aircraft. Chemical composition of the wing panel alloy and of the pristine material are given in Table 2. One can observe differences in chemical composition between the wing panel alloy and the pristine material, in particular for the copper content. However, Shih et al. [12] showed that, for 2024 aluminium alloy, the major parameter for the precipitation of S' phase was the value of a pre-aging strain and not the alloying contents. Further, Richard et al. [13] studied the fatigue behaviour of 2022 and 2024 alloys. They showed that the two alloys presented a similar fatigue behaviour in the propagation step despite of their differences in copper content. Therefore, it was assumed here that the different samples, i.e. wing panel samples and pristine samples, could be compared.

As regards more precisely the material aged under actual service condition, the work presented here was concerned with the intrados panels of the A320 aircraft with the Manufacture Serial Number MSN004. This aircraft was operated for 38 637 flights (35 342 hours) over 21 years. The material constitutive of the intrados panels is a 2024 aluminium alloy; it had been introduced in the T351 metallurgical state, i.e. solution heat treatment at 495

°C (+/- 5 °C), water quenching, straining and then tempering at room temperature for 4 days. Two zones of the wing, shown in Figure 1, were examined. The first one was located at the tip of the wing (samples designated as W_T) and did not endure severe mechanical loading while the second area, which was placed close to the engine (samples called as W_E), was assumed to sustain higher mechanical loading and maybe exposure to higher temperatures susceptible to generate microstructural modifications. The samples were taken from the plane of the aircraft wing at a considerable distance from the panel fixation in order to avoid the effect of cold expansion at the riveting points.
The wing panels under study were originally fabricated from laminated plates, in such a manner that the longitudinal orientation of the grains is collinear with the longitudinal direction (L) of the wing. Optical observations of the wing panels after Keller's etching revealed grains elongated in the longitudinal direction; a strong heterogeneity was noticed in the grain sizes, with dimensions varying from 100 µm to 1 mm in the longitudinal direction.

2.2 Characterization of the microstructure and of the fracture surface

Optical microscope (OM) observations of both wing panels and pristine materials revealed the presence of coarse intermetallic particles. Observations carried out with a field emission gun scanning electron microscope (FEG SEM-7000F from JEOL with the incident electron beam maintained between 10 kV and 15 kV) combined with analyses performed with an SDD Bruker X flash energy dispersive X-ray spectrometer (EDX) allowed the coarse intermetallic particles to be more accurately characterized and analyzed. SEM observations were also used for the analysis of the fracture surface obtained after tensile tests and fatigue tests (see below) for the samples from pristine, artificially aged and wing panel material.
Concerning the microstructure, transmission electron microscope (TEM) observations from a JEOL-JEM-2010 were also performed to characterize the fine precipitation, i.e. hardening precipitates. The samples were obtained by removing 300 µm thick slices from the wing panels or the artificially aged pristine material. The slices were ground down to approximately 100 µm thick and a dimple was machined in the central region. Final electron transparency was obtained by ion milling on a precision ion polishing system (PIPS(tm), Gatan) using 5 kV Ar^+ ions.

2.3 Conductivity measurements

Conductivity measurements were performed by using an Elotest B300 apparatus combined with a CSCAN mapping software. The evaluation of the conductivity was based on Foucault current measurements. Before testing the samples, the apparatus was calibrated using three reference samples with conductivity equal to 17.1, 21.1 and 24 MS $\times$ m^{-1}, respectively. The sample geometry was similar to that of the reference samples, i.e. 4 $\times$ 4 $\times$ 5 mm^3 parallelepipeds. Frequency was fixed at 30 kHz in order to achieve a penetration depth around 1 mm. At least 5 measurements were performed for each sample to check the reproducibility of the data. Mean values are given; the scattering of the results was no more than 0.1 MS$\times$ m^{-1}.

2.4 Characterization of the mechanical properties

Macrohardness measurements were first performed to evaluate the ageing of the wing panels by comparison with the results obtained from the artificially aged samples of pristine alloy. Vickers measurements were performed using a 30 kg loading. For each sample, at least three

measurements were performed. Mean values are given and error bars are added on the corresponding graph.
Tensile tests were carried out using conventional flat tensile specimens (ASTM E8) with a gauge length equal to 32 mm (Figure 2a) at a constant strain rate of 10^{-3} s^{-1}on an Instron testing machine equipped with an extensometer and a 5 kN load cell. For each sample, at least 3 tensile tests were performed. Mean values are given and error bars are added on the corresponding graph. Two loading directions, namely longitudinal (L) and transverse (T), were tested. As often observed in rolled plates, small differences in the strength characteristics were shown in the longitudinal direction compared to the perpendicular direction but there were assumed to be not significant. Further, comparison of the tensile properties between the pristine material, the aged samples and W_E and W_T samples for both directions led to the same conclusions. Therefore, for brevity, we chose to give here only the results for the L direction. Fracture surfaces were characterized after test completion.
The influence of ageing on fatigue life was determined by first establishing S-N curves on the pristine and the wing materials, and then by assessing the fatigue lives as a function of artificial ageing conditions at selected values of the maximum stress. Tests were conducted on flat dogbone (Airbus type, referred to FPE 5A) 3mm thick specimens (Figure 2b). All the external surfaces were prepared by mechanical polishing down to 1 micron in order to prevent premature initiation from surface defects, so as not only ensure reproducibility of test results, but also provide conditions for a proper comparison between different ageing conditions. Tests were carried out in laboratory air at room temperature under a load ratio of 0.1 until failure. Five stress levels were selected, namely: 250, 275, 300, 350, and 400 MPa. Two loading directions, namely longitudinal (L) and transverse (T), were also tested to examine the possible influence of the orientation. The fatigue data were furthermore analysed on the basis of SEM observations of the fracture surfaces and of calculations using the AFGROW software [14].

3. Results

3.1 Microstructure and physical property (conductivity) evolution under different artificial ageing

First, artificially aged pristine samples were observed by OM before and after a Keller's etching. As expected, no evolution was observed concerning both the coarse intermetallic particles and the grain sizes. SEM observations (Figure 3) and EDS analyses did not allow to evidence any significant differences concerning the coarse intermetallic particles except a strong reactivity of the coarse intermetallics/matrix interface for ageing treatment duration as long as or longer than 80 h. This particular behavior was revealed due to the formation of a deep trench around the coarse particles for long ageing treatments, which was not observed in ageing treatments shorter than 80 h, even if the surface preparation for SEM observations was strictly controlled and similar from one sample to another. This result suggests a modification of the chemical composition of the coarse particles or of the surrounding matrix when the duration of the ageing treatment is increased. SEM observations of samples from the wing panels show that, for W_T samples, the coarse intermetallic particles are characteristic of those commonly found in a 2024 T351 alloy with Al_2Cu, Al_2CuMg, Al-Cu-Mn-Fe coarse particles; no reactivity of the intermetallics/matrix interface is noticed. Concerning W_E samples, the same types of intermetallic particles were observed with no strong reactivity of the intermetallics/matrix interface; however, large clusters of coarse particles are observed as well as a fine intragranular precipitation.

To go further, TEM observations were carried out for both artificially aged samples from pristine material and samples from wing panels (Figure 4). Figure 4a shows that intergranular precipitates were observed as expected for any 2024 T351 alloy. They were identified in previous works as Al-Cu-Mg and Al-Cu-Mn precipitates [15,16]. No intragranular precipitation was observed. The comparison of Figures 4a, b, c and d indicates that, when the ageing duration is increased, intergranular precipitates become larger and more numerous so that they form a continuous precipitation path after 177h at 150 °C. Moreover, acicular intragranular precipitates were observed from 55h of ageing treatment; their size increased when the ageing duration increased. Acicular intragranular precipitates were identified as hardening S' (Al,Cu,Mg) precipitates. The formation of intragranular hardening precipitates was correlated with a decrease of the Cu content of the solid solution. This could explain the reactivity of the intermetallic/matrix interface previously observed by SEM (Figure 3). For the 177 h ageing treatment, a precipitate free zone (PFZ) is also observed, which is consistent with the growth of the Cu-rich intergranular precipitates. TEM observations of W_T samples (Figure 4e) showed that the microstructure of the wing panel far from the engine was similar to that of the 2024 T351 sample. On the contrary, Figure 4f shows the presence of large intergranular precipitates and intragranular hardening precipitates for W_E samples; this observation indicates that a significant microstructural ageing occurred in this condition, probably due to the exposure to higher temperatures than for the W_T material during the service life, but also presumably due to the higher mechanical loading in this area. Indeed, several authors showed that the precipitation kinetics is influenced by a deformation [17]. Qualitative comparison of Figures 4a, b, c, d and Figure 4f suggests that the metallurgical state induced by ageing in W_E samples corresponds to a 55h artificially aged pristine material.

Conductivity measurements were helpful in quantifying the ageing stage of the wing panels. Indeed, Figure 5 shows that, for ageing duration from 0 to 55h, the conductivity of the 2024 alloy remains nearly stable: indeed it slowly increases from 17 to 17.5 $MS.m^{-1}$. From 55h of artificial ageing, a sharp increase of the conductivity is observed with values reaching 20 $MS.m^{-1}$ for a 177h ageing treatment. This variation in the conductivity as a function of the ageing duration is consistent with the microstructural evolution previously described. Altogether these results evidence a significant modification of the microstructure for ageing duration longer than 55h. Conductivity measurements performed on the wing panels lead to values between 17.15 and 17.32 $MS.m^{-1}$ for W_T samples and 17 and 17.3 $MS.m^{-1}$ for W_E samples. The results confirm that the microstructure of both W_T and W_E samples correspond to ageing treatment durations lower than 55h, which is consistent with the equivalence time-temperature initially assumed (Table 1) to design the ageing treatments.

3.2 Effect of artificial ageing on static mechanical properties

3.2.1 Hardness measurements

Macrohardness measurements performed for artificially aged samples (Figure 6) lead to the same conclusions concerning the kinetics of the ageing at 150°C in the 2024 T351 alloy. Indeed, from 0 to 55h of ageing at 150°C, the hardness values remain quite stable and lower than 135 HV while, starting from 55h of ageing duration, the hardness values strongly increase to reach 160 HV for a 177h ageing treatment. These results are consistent with the TEM observations indicating a significant microstructural evolution from 55h of ageing treatment at 150°C. Measurements performed for the wing panels provide hardness values between 136 and 140 HV for W_T samples, and 138 and 143 HV for W_E samples. Taking into

account the differences in chemical composition between the pristine material and the wing panels, it was assumed that the hardness values measured for the wing panels, independent of the location of the samples (near or far from the engines), correspond with an ageing lower than a 55h exposure at 150°C, in agreement with the TEM observations. The results are consistent with literature data [4,18,19]

3.2.2 Residual tensile properties

Figure 7 presents the residual tensile properties measured for pristine material after artificial ageing at 150 °C. Maximum stress, yield stress and elongation to failure were considered as the main parameters characteristic of the microstructural evolutions. As expected from the previous results, these three parameters are quite constant from 0 to 55h of ageing treatment, except a small decrease in the elongation to failure measured for the 55 h aged pristine sample. On the contrary, from 55h of ageing treatment, the yield stress sharply increases, consistently with the large precipitation of hardening precipitates noticed in Figure 4. Simultaneously, the elongation to failure decreases as expected. No significant variation of the maximum stress is noticed. The results indicate that the mechanical properties measured for the 177h aged samples are similar to those obtained by Kaufman [20] for a 2024 T81 alloy. Moreover, according to literature [20,21], in aluminium alloys, an ageing treatment induces an increase of the yield stress and a decrease of the elongation to failure, but with no significant modification of the ultimate tensile strength. Tensile properties determined for the wing panels are also reported in Figure 7. For W_T samples, it can be observed that yield stress and elongation to rupture are quite similar to the values measured for the 2024 T351 pristine material. In W_E samples however, more significant variations of the tensile properties compared to the 2024 T351 pristine material are noticed. Thus, the yield stress values of W_E samples are close to those obtained in a 80h aged material, while the elongation to failure values allowed to estimate the ageing between 55h and 80h at 150 °C, corresponding to an equivalent treatment duration at 80°C a little bit higher than 100 000 h (Table 1), which corresponds with the actual aircraft service life. The comparison of mechanical properties between the pristine material and wing panel alloy might be skewed by a discrepancy in initial chemical composition. Nevertheless, the results clearly indicate a difference in ageing between W_E and W_T samples; the differences were consistent with the location of the samples in the aircraft. Furthermore, considering the different results collected, i.e. TEM observations, conductivity and hardness measurements, and finally tensile properties, the difference in aging between W_E and W_T samples is clear, with the W_E aging conditions corresponding to a treatment at 150°C for about 55h.

3.2.3 Fracture surface analysis

Figure 8 presents the fracture surface observed by SEM after the tensile tests. In the pristine 2024 T351 alloy, a ductile fracture surface is observed with the presence of voids (Figure 8a). When the alloy is aged at 150°C, for duration shorter than 55 h, no significant modification of the fracture surface is observed. In the 55h aged material however, while fracture is still mainly ductile, two types of voids can be distinguished (Figure 8b). The first type presents a size similar to that observed in the pristine 2024 T351 alloy; it is associated to the presence of coarse intermetallic particles as often observed in the literature [4]. The second type of voids, i.e. microvoids with a diameter around 500 nm, might be associated to the intragranular hardening precipitation as observed by TEM (Figure 4). For ageing times equal to or longer than 80 h, the fracture surface is mainly ductile, with the presence of the two types of voids

previously described; however, it also evidences characteristic features corresponding with intergranular fracture, probably due to the coalescence of microvoids located in the grain boundary vicinity (Figure 8c). The occurrence of intergranular fracture is more pronounced when the duration of the ageing treatment is prolonged. This is attributed to the presence of numerous intergranular precipitates induced by long duration ageing treatments (Figure 4) which enhances the coalescence of microvoids under mechanical stress. SEM observations of the fracture surface of W_E and W_T samples confirm a difference between the two in ageing conditions. Indeed, in W_T samples (Figure 8e), the fracture surface is similar to that obtained for the 2024 T351 alloy after short ageing durations; in W_E samples however, some intergranular fractures are observed as for longer ageing durations. Considering that these features are rarely observed in W_E samples, it is assumed that these samples reflect an ageing treatment ranging between 55 and 80h in agreement with previous conclusions.

3.3 Effect of actual and artificial ageing on fatigue resistance

3.3.1 Fatigue life

The results of fatigue tests carried on pristine, W_E and W_T materials are presented in Figure 9. For a selected value of the maximum stress, no significant difference in fatigue life can be noticed between the pristine material and the alloy aged under actual service conditions. The same observation stands for the influence of orientation in a given material. However, in order to take into account the differences in strength noticed in tensile tests, these fatigue data are also plotted by dividing the maximum stress by the yield strength. This representation does not fundamentally modify the picture and it is difficult to state about a possible effect of ageing on fatigue resistance.

The results of fatigue test obtained on artificially aged material are presented in Figure 10a. For a selected maximum stress level, no significant difference in fatigue life is noticed for the different ageing conditions under consideration. It seems however that artificial ageing at t_{177} somehow reduces the fatigue life. Indeed the number of cycles to failure N decreases from an average value of 95 006 cycles (t_0, t_{27} and t_{55}) down to 71 587 cycles (t_{177}), reflecting a 25% reduction in life. It should be reminded that, as shown in the previous sections, the microstructural changes induced by ageing result into variations in mechanical properties. In particular the t_{177} heat treatment corresponds with a significant increase in yield strength. It could be expected that an increase in strength may also result in an improvement in fatigue strength. Therefore, in order to take into account these differences in strength, the same data are plotted in Figure 10b by dividing the maximum stress by the corresponding 0.2% yield strength determined on the same specimen geometry. By using this method, a relative degradation in fatigue resistance of the t_{177} condition is revealed. Indeed, as the tensile resistance is higher, a higher fatigue resistance might be expected, provided that the initiation and propagation mechanisms are not fundamentally altered. In order to confirm this trend, additional stress levels were tested for this ageing condition. The results reported in Figure 10b do confirm this relative degradation in fatigue resistance.

The results of fatigue tests performed for the wing panels (W_T) are also reported in Figure 10a. For a selected value of the maximum stress, no significant difference in fatigue life can be noticed between the artificially-aged pristine material and the alloy aged under actual service conditions. The same observation stands for the influence of orientation in a given material (not shown here). As previously done for aged pristine materials, in order to take into account the differences in strength noticed in tensile tests, these fatigue data are modified by dividing the maximum stress by the yield strength (Figure 10b). The results indicate that it is

difficult to state about a possible effect of actual ageing on fatigue resistance. Conclusions are similar for W_E samples as previously shown in Figure 9.

3.3.2 Fracture surfaces

Observations of the fracture surface in the vicinity of initiation sites are reported in Figure 11 for different artificial ageing with nearly the same magnification. In any case, a predominance of a stage II, cleavage-like fracture mode, is noticed. However some crystallographic facets, reminiscent of a stage-I like propagation regime [22], were also present on the fracture surfaces in the case of t_0 to t_{55} heat-treatments. Typical examples are presented in Figure 12 for a maximum stress of 300 MPa. Additional tests performed at higher stress levels indicate a lower fraction of such facets. It seems that these facets were less numerous as the ageing treatment is prolonged. Thus, for an ageing condition corresponding with 3 times the aircraft service life, namely the t_{177} heat treatment, such facets were no longer observed. Interestingly, such facets are also present in the material aged in actual W_E and W_T conditions (Figure 11d), which is consistent with the observations on artificially aged material. This suggested that the absence of these facets could be interpreted as a signature of ageing, while the detailed mechanisms responsible for the localisation of the deformation associated with this particular fracture mode still needed to be detailed. The formation of crystallographic facets can be accounted by the heterogeneity of deformation induced by the precipitation structure. At ageing condition t_{177}, the associated evolution of microstructure would be reflected by the disappearance of crystallographic facets which could thus be used as an indicator for service life ageing aircraft structure. This would need to be confirmed, in particular by quantitative measurements of the relative area occupied by such facets as a function of ageing.
SEM observations of the stable propagation area prior to final failure were also carried out. Typical views are shown in Figure 13a to f. The location of the different observations is more precisely indicated in Figure 13a in the case of the material aged for 27h at 150°C and subsequently fatigue with σ_{max}=300MPa. It can be seen that striations are present from point 1 to point 3. However the striation spacing is larger in point 3 (Figure 13d). In areas 3, 4, and 5 which are close to final fracture, while striations are still present, the fracture mode becomes more ductile as indicated by the presence of dimples. The measurement of striation spacing permits a determination of the local growth rate. These data are discussed in the next section.

3 Analysis and discussion

SEM/TEM observations, conductivity measurements and tensile results all indicate that two steps could be considered in the ageing of the 2024 alloy at 150°C with a critical time around 55h. Indeed, for ageing durations shorter than 55h, no significant evolution of the microstructure is observed; the conductivity and the mechanical properties of the alloy remain nearly stable with a ductile fracture surface as expected. From 55h, a marked increase is noticed in the kinetics of hardening precipitation combined with the growth of intergranular precipitates. As a consequence, the elongation to failure significantly decreases while the yield stress strongly increases. The fracture surface examination evidences characteristic features associated to intergranular rupture. The comparison of the results obtained with the aged pristine samples and wing panel specimens indicates that the ageing of the wing panel material corresponds with an ageing duration between 55h and 80h at 150°C, i.e. an ageing condition equivalent to less than 145 000 h at 80°C, depending on the location of the samples on the aircraft.

Concerning the fatigue results, they indicate no clear influence of ageing conditions on the fatigue resistance. However this situation could result from a different balance between the initiation stage and the propagation stage as a function of microstructural modification induced by ageing. It is noteworthy that a study of fatigue crack growth resistance indicated no difference in growth rates between the pristine alloy and the material aged on the aircraft wing [23], which suggests that, provided that the initial flaw size as well as the critical crack depth are not fundamentally modified, the propagation life should not be different either. Given this information, and in order to analyse the fatigue data as a function of ageing, fatigue life predictions were performed for the specimens tested using the AFGROW fracture-mechanics software [14]. The initial crack was modelled using the centre semi-elliptic surface flaw model, where a_0 and c_0 are the initial flaw sizes, submitted to a tension stress. The fatigue life predictions were conducted by using the parameters of NASGRO equation for the 2024 T351 alloy. Indeed additional fatigue crack growth test results revealed a good agreement between this law and experimental data on pristine and aged material [23]. The methodology used was derived from the Equivalent Initial Flaw Size (EIFS) as introduced by Johnson [24]. Basically the initial flaw sizes were adjusted so that the prediction of propagation life fitted with experimental number of cycles to failure. The values of a_0 and c_0 thus obtained could be compared to estimation of the initial flaw size from fracture surface observations. Alternatively, these experimental measurements could be used as input data in computations using the same crack growth law to predict a fatigue life. Furthermore, in order to get higher confidence in the computations, striation spacing measurements were compared to the predicted growth rates at different crack depths in Figure 14. It can be seen that the predictions are in agreement with experimental data, except for crack depth larger than 1.5 mm. It also appeared that local crack growth rates, for a given crack depth, are nearly the same regardless of the applied ageing treatment. The results of these investigations for 12 specimens of artificially aged material (3 specimens of t_0, t_{27}, t_{55} and t_{177}) as well as material from the teardown in the engine area all fatigued with a maximum stress of 300 MPa are summarised in Table 3. Once again, regardless of the estimation procedure considered, no clear trend could be observed in the initial flaw dimensions which are in the range 30 µm-100 µm, including the data pertaining to the material aged under actual service conditions in the wing tip as in the engine area. Clearly, additional data are required to gain a statistical view of the initial flaw size as a function of ageing. Nevertheless, these data will be useful for the analysis of the fatigue life of pre-corroded specimens where the initial flaw is assumed to be the corrosion defect. This analysis will be published in a companion paper.

4 Conclusions

The impact of long-time thermal exposure on microstructural changes and associated residual mechanical properties of a 2024-T351 aluminium alloy was here investigated by considering an initially pristine alloy which was subsequently artificially aged and a material from the teardown of wing panels of a decommissioned A320 aircraft. The results of the fatigue tests do not bring to the fore any significant impact of thermal ageing on the residual fatigue resistance for ageing conditions corresponding with a service life. Indeed the fatigue lives of the alloy aged during 55h at 150°C as well as the material issued from the teardown are comparable to the data obtained on a pristine alloy in the stress range under consideration. Furthermore the analysis of fracture surface associated with fracture mechanics computations indicate that the similitude in fatigue lives does not result from a different balance in initiation and propagation stages as a function of ageing, despite of the differences observed in microstructure. However it is also shown that the hardening induced by longer ageing conditions (177h at 150°C) does not correspond with a superior fatigue resistance, which

suggests that a modification in fatigue mechanisms has been initiated. This has to be paralleled with the microstructure observations and the conductivity measurements, despite the absence of any salient change in fracture mode as observed during tensile test.
Finally, while the results presented here do not evidence any significant degradation of mechanical performances of the alloy at the end of the service life, the microstructural modifications may also influence the corrosion resistance, which in turn can affect the structural integrity. This issue was also addressed in the framework of the present study and will be presented in a companion paper.

References

[1] N. D. Alexopoulos, Z. Velonaki, C. I. Stergiou, and S. K. Kourkoulis, Effect of ageing on precipitation kinetics, tensile and work hardening behavior of Al-Cu-Mg (2024) alloy, Materials Science and Engineering: A 700 (2017) 457-467.

[2] G. Harlow and R. P. Wei. Materials aging and structural reliability in, 6th Issat International Conference on Reliability and Quality in Design, Proceedings, INT SOC SCI APPL TECHNOL, Piscataway, 2000; pp. 1-6.

[3] A. May, M. A. Belouchrani, S. Taharboucht, and A. Boudras. Influence of heat treatment on the fatigue behaviour of two aluminium alloys 2024 and 2024 plated in, Fatigue 2010, 2010; pp. 1795-1804.

[4] D. A. P. Reis, A. A. Couto, N. I. Domingues, Jr., A. C. O. Hirschmann, S. Zepka, and C. Moura Neto. Effect of Artificial Aging on the Mechanical Properties of an Aerospace Aluminum Alloy 2024 in: A. Ochsner, G.E. Murch, A. Shokuhfar, and J. Delgado (Eds.), Diffusion in Solids and Liquids Vii, 2012; pp. 193-198.

[5] R. A. Everett, Effects of service usage on tensile, fatigue and fracture properties of 7075-T6 and 7178-T6 aluminium alloys. National Aeronautic and Space Administration, NASA Langley Research Center, Hampton, Va, 1975.

[6] J. N. Scheuring and A. F. Grandt, Mechanical properties of aircraft materials subjected to long periods of service usage, Journal of Engineering Materials and Technology-Transactions of the Asme 119 (1997) 380-386.

[7] J. J. Gruff and J. G. Hutcheson, Effects of corrosive environments on fatigue life of aluminium alloys under maneuver spectrum loading. Defense Technical Information Centre, 1969.

[8] E. M. Nicht, G. Brauer, and G. Tempus, Long-time aging behaviour of the alloy Al-2024 characterized by positron annihilation spectroscopy, Acta Physica Polonica A 99 (2001) 441-445.

[9] V. N. Basov, G. I. Nesterenko, B. G. Nesterenko, and V. G. Petrusenko, Study of deterioration of the material properties during aircraft operation, Strength of Materials 38 (2006) 398-403.

[10] F. Menan and G. Henaff, Influence of frequency and exposure to a saline solution on the corrosion fatigue crack growth behavior of the aluminum alloy 2024, International Journal of Fatigue, 31 (2009) 1684-1695.

[11] I. N. Khan and M. J. Starink, Mircostructure and strength modelling of Al-Cu-Mg alloys during non-isothermal treatments: Part 1 - Controlled heating and cooling, Materials Science and Technology 24 (2008) 1403-1410.

[12] H. C. Shih, N. J. Ho, and J. C. Huang, Precipitation behaviors in Al-Cu-Mg and 2024 aluminum alloys, Metallurgical and Materials Transactions a-Physical Metallurgy and Materials Science 27 (1996) 2479-2494.

[13] S. Richard, C. Gasqueres, C. Sarrazin-Baudoux, and J. Petit, Coupled influence of microstructure and atmosphere environment on fatigue crack path in new generation Al alloys, Engineering Fracture Mechanics 77 (2010) 1941-1952.

[14] J. A. Harter, AFGROW users guide and technical manual (http://www.siresearch.info), Wright-Patterson Air Force Base OH 45433-7542, 2006.

[15] C. Larignon, J. Alexis, E. Andrieu, L. Lacroix, G. Odemer, and C. Blanc, Combined Kelvin Probe Force Microscopy and Secondary Ion Mass Spectrometry for Hydrogen Detection in Corroded 2024 aluminium alloy, Electrochimica Acta 110 (2013) 484-490.

[16] C. Larignon, J. Alexis, E. Andrieu, G. Odemer, and C. Blanc, Propagation of intergranular corrosion defects in AA 2024-T351 evaluated by a decrease in mechanical resistance, Journal of the Electrochemical Society 161 (2014) C339-C348.

[17] A. Deschamps, F. de Geuser, Z. Horita, S. Lee, and G. Renou, Precipitation kinetics in severely plastically deformed 7075 aluminium alloy, Acta Materialia 66 (2014) 105-117.

[18] A. Cochard, K. Zhu, S. Joulie, J. Douin, J. Huez, L. Robbiola, P. Sciau, and M. Brunet, Natural aging on Al-Cu-Mg structural hardening alloys - Investigation of two historical duralumins for aeronautics, Materials Science and Engineering a-Structural Materials Properties Microstructure and Processing 690 (2017) 259-269.

[19] T. R. Prabhu, Effects of ageing time on the mechanical and conductivity properties for various round bar diameters of AA 2219 Al alloy, Engineering Science and Technology, an International Journal 20 (2017) 133-142.

[20] J. G. Kaufman,Properties of aluminium alloys: tensile, creep, and fatigue data at high and low temperatures: ASM International, Materials Park, Ohio, 1999.

[21] N. D. Alexopoulos, On the corrosion-induced mechanical degradation for different artificial aging conditions of 2024 aluminum alloy, Materials Science and Engineering a-Structural Materials Properties Microstructure and Processing 520 (2009) 40-48.

[22] J. Petit, G. Henaff, and C. Sarrazin-Baudoux, Mechanisms and modeling of near-threshold fatigue crack propagation, Fatigue Crack Growth Thresholds, Endurance Limits, and Design ASTM STP 1372 1372 (2000) 3-30.

[23] F. Billy, G. Hénaff, G. Benoit, and S. Van der Veen, Residual Fatigue Properties of a 2024-T351 Aluminium Alloy from the Teardown of AIRBUS A320 Wing Panels after Service. 11th International Fatigue Congress, Fatigue 2014, Melbourne, Australia, G. Clark and C.H. Wang G. Clark and C.H. Wangs. Advanced Materials Research, 2014, pp. 621-626.

[24] W. S. Johnson. The history, logic and uses of the Equivalent Initial Flaw Size approach to total fatigue life prediction in, Fatigue 2010, Elsevier Science BV, Amsterdam, 2010; pp. 47-58.

Captions of figures and tables

Tables

Table 1: Artificial ageing time of 2024-T351 aluminium alloy at 150 °C, equivalent to aircraft ageing life at 80° C. Grey colour = service life of the aircraft.

Table 2: Chemical composition of the wing panels and of the pristine material (wt. %)

Table 3: Computed and experimental initial flaw sizes, predicted and experimental fatigue life at different artificial ageing conditions.

Figures

Figure 1: Areas of interest in the wing panels from the A320 MSN004 aircraft.

Figure 2: Geometry of the samples for mechanical tests (a) tensile tests (b) fatigue tests.

Figure 3: SEM micrographs, L-T sections of 2024-T351, at different ageing times at 150 °C: (a) t_0, (b) t_{55} (c) t_{80} (d) t_{177} (e) W_T sample (f) W_E sample.

Figure 4: TEM micrographs of L-T sections of 2024-T351 at different ageing times at 150 °C (a) t_0, (b) t_{55} (c) t_{80} and (d) t_{177} (e) W_T sample (f) W_E sample.

Figure 5: Electric conductivity as a function of artificial ageing time at 150°C. Results for wing panels are reported for comparison.

Figure 6: Macrohardness as a function of artificial ageing time at 150°C for 2024 alloy. Results for wing panels are reported for comparison.

Figure 7: Relative tensile properties as a function of artificial ageing time at 150°C, data normalised with tensile properties for a 2024 T351 alloy. Results for wing panels are reported for comparison.

Figure 8: SEM micrographs, S-T fracture plane, of 2024-T351 at different ageing times at 150 °C: (a) t_0 (b) t_{55} (c) t_{80} and (d) t_{177}. Results for wing panels are reported for comparison: (e) W_T sample (f) W_E sample.

Figure 9: S-N curves of W_E and W_T in longitudinal and transverse directions compared to data obtained on a pristine material (a); same data as in (a) with the maximum stress divided by the yield strength of the material (b).

Figure 10: S-N curves of different artificial ageing as compared to the wing and pristine material (a) σ_{max} versus the number of cycles to failure (b) σ_{max} divided by the 0.2% yield stress versus the number of cycles to failure.

Figure 11: SEM images of the crack initiation site at different ageing durations at 150°C: (a) t0, (b) t_{27}, (c) t_{177} and (d) actual ageing in aircraft wing tip W_T (σ_{max} =300MPa).

Figure 12: Crystallographic facets observed at (a, b) t_0 (c) t_{27} and ageing aircraft wing (σ_{max}=300MPa).

Figure 13: (a) General view of a typical fracture surface (aged 27h/150°C – σ_{max} =300MPa) where the arrow and numbers represent the vector and positions along which striation measurements were performed; (b) striations in location 1; (c) striations in location 2; (d) striations in location 3; (e) striations in location 4 and (f) striations in location 5.

Figure 14: Fatigue crack growth rate versus crack depth from the initiation site. Symbol represents crack progression along a vector in Figure 10 (a). Data included AFGROW prediction in dashed lines at different artificial ageing.

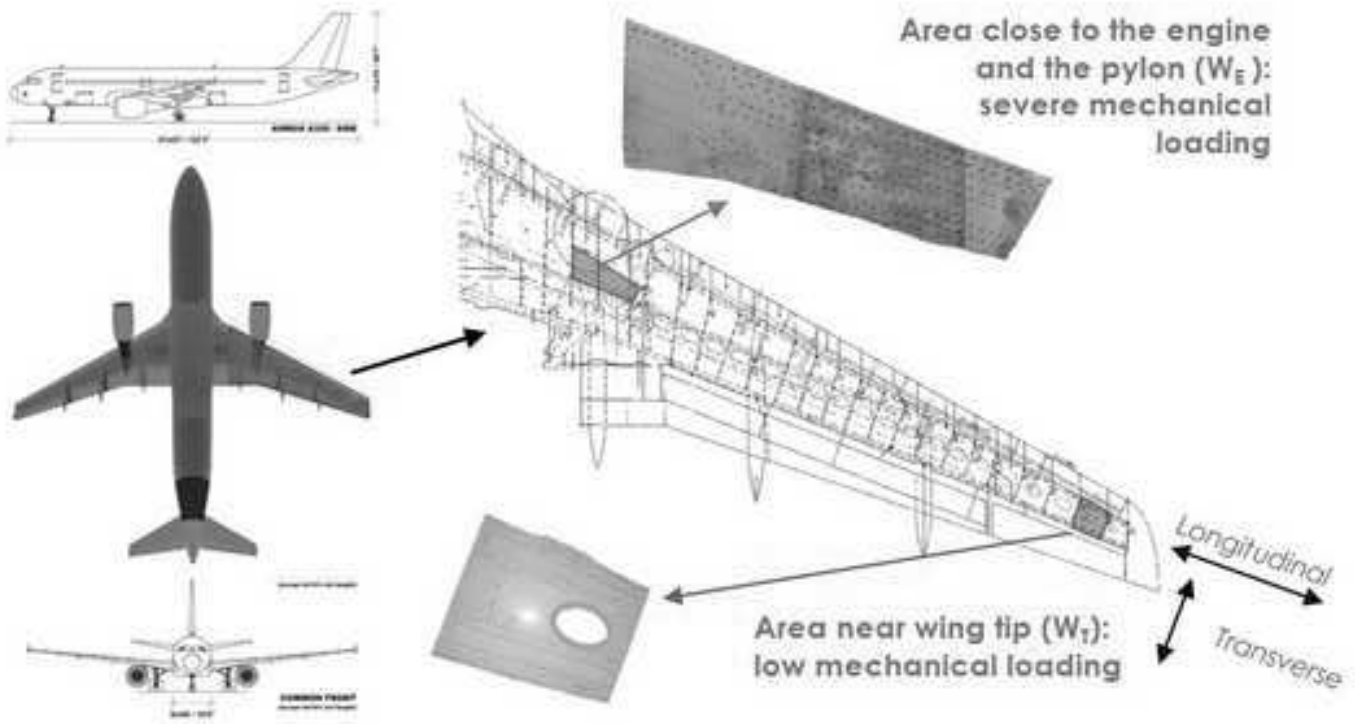
Area close to the engine and the pylon (W_E): severe mechanical loading
Area near wing tip (W_T): low mechanical loading
Longitudinal
Transverse

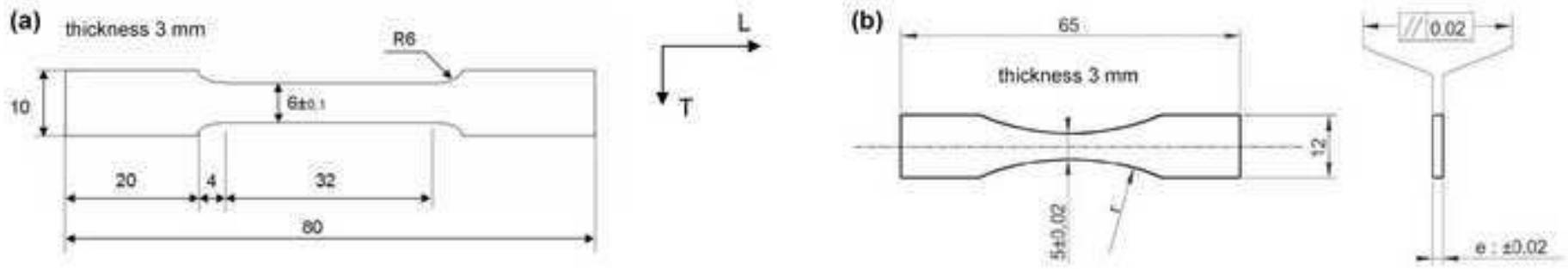
(a)
thickness 3 mm
R6
10
6±0.1
20
4
32
80
L
T
(b)
65
thickness 3 mm
12
5±0.02
r
// 0.02
e : ±0.02

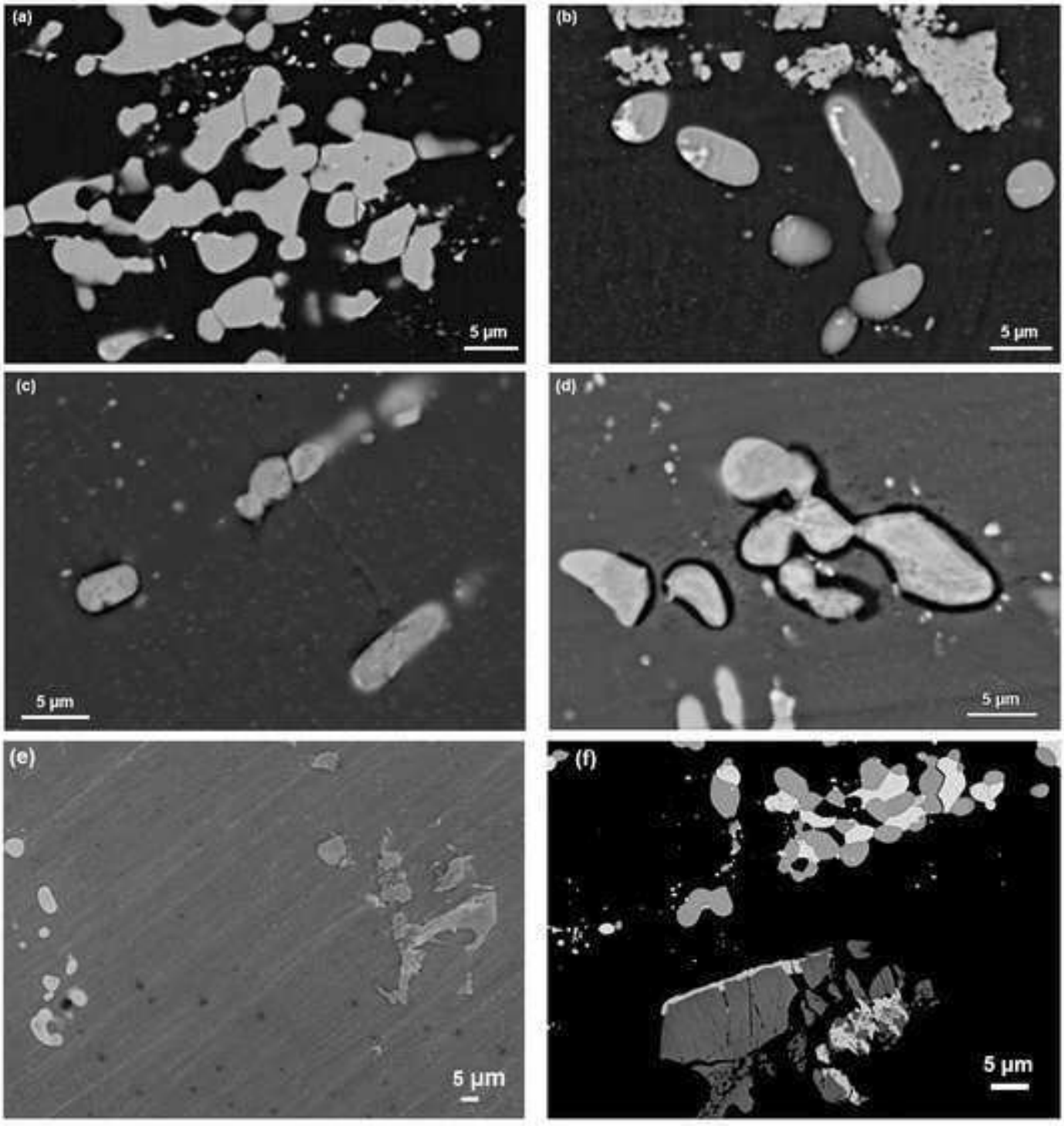
(a)
5 µm
(b)
5 µm
(c)
5 µm
(d)
5 µm
(e)
5 µm
(f)
5 µm

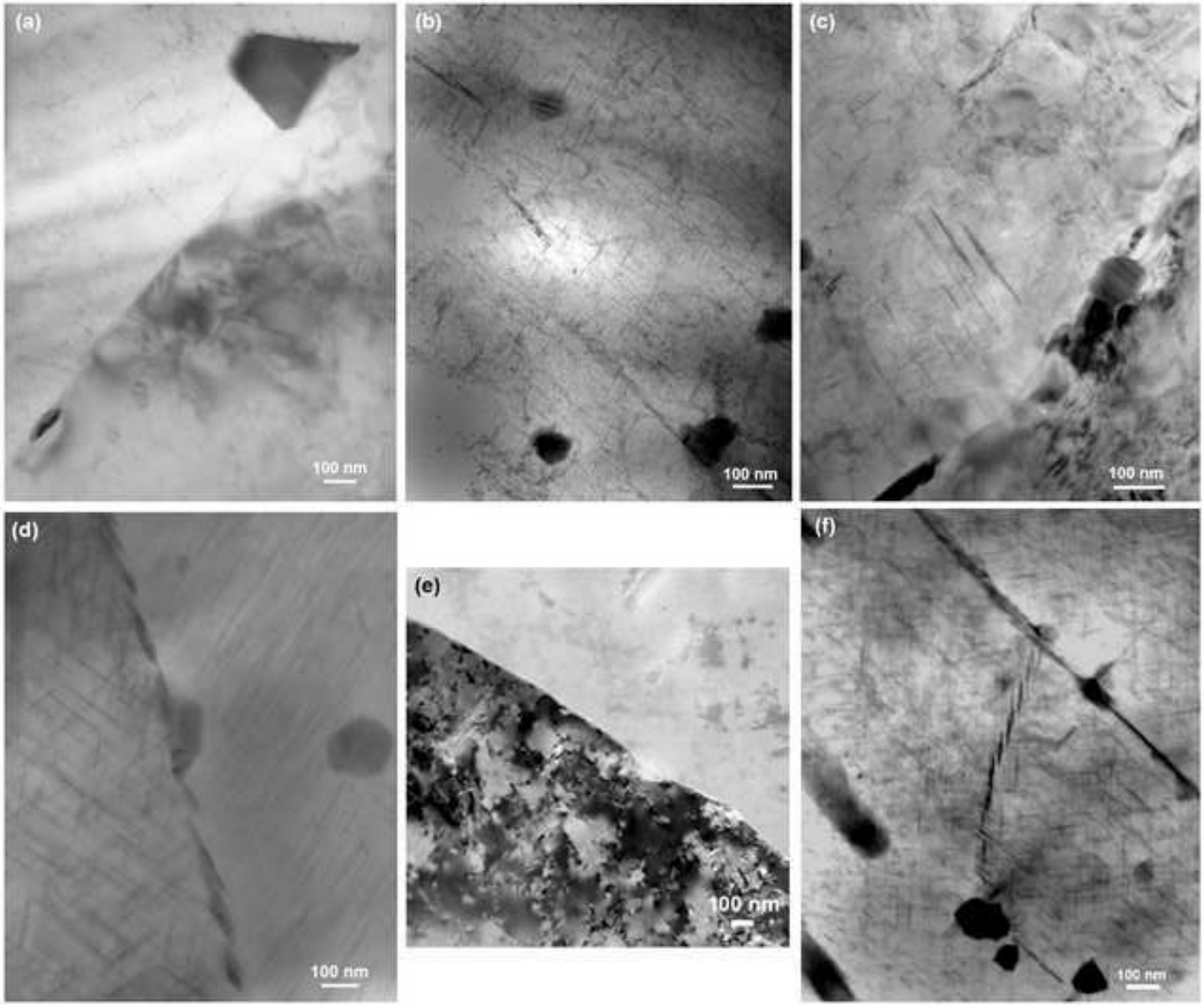
(a)
100 nm
(b)
100 nm
(c)
100 nm
(d)
100 nm
(e)
100 nm
(f)
100 nm

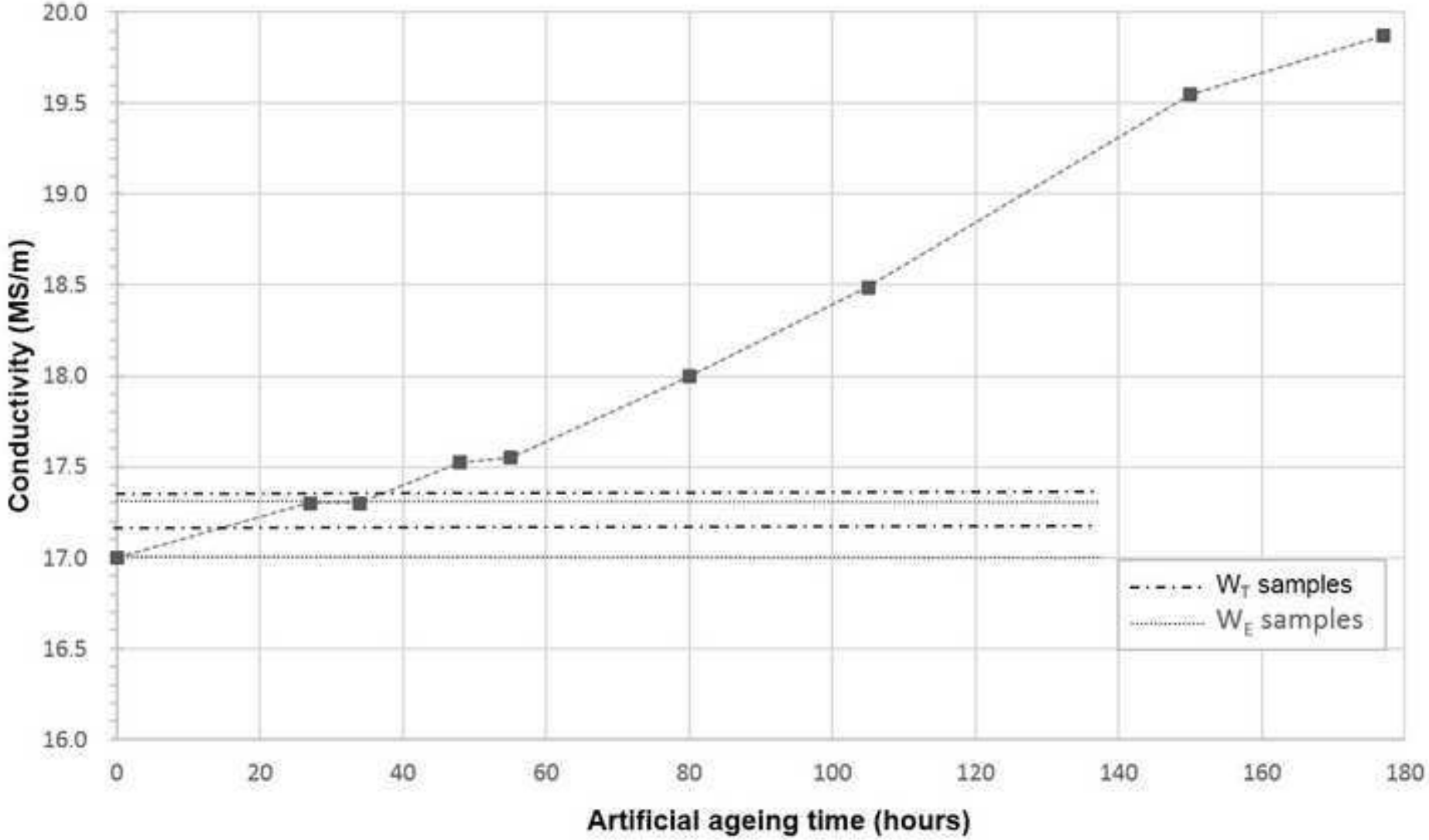
20.0
19.5
19.0
18.5
18.0
17.5
17.0
16.5
16.0
Conductivity (MS/m)
0
20
40
60
80
100
120
140
160
180
Artificial ageing time (hours)
W_T samples
W_E samples

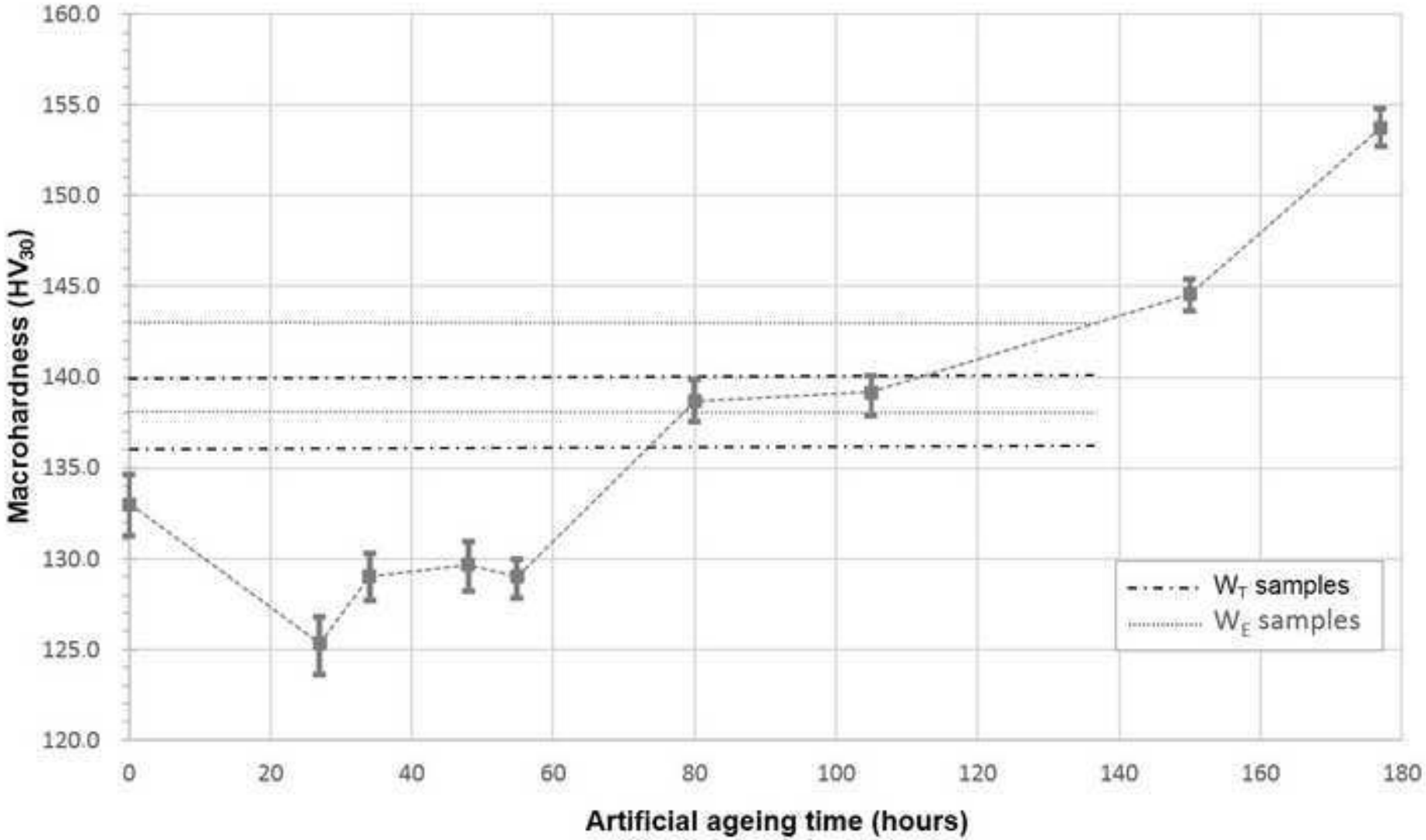
160.0
155.0
150.0
145.0
140.0
135.0
130.0
125.0
120.0
Macrohardness (HV30)
0
20
40
60
80
100
120
140
160
180
Artificial ageing time (hours)
WT samples
WE samples

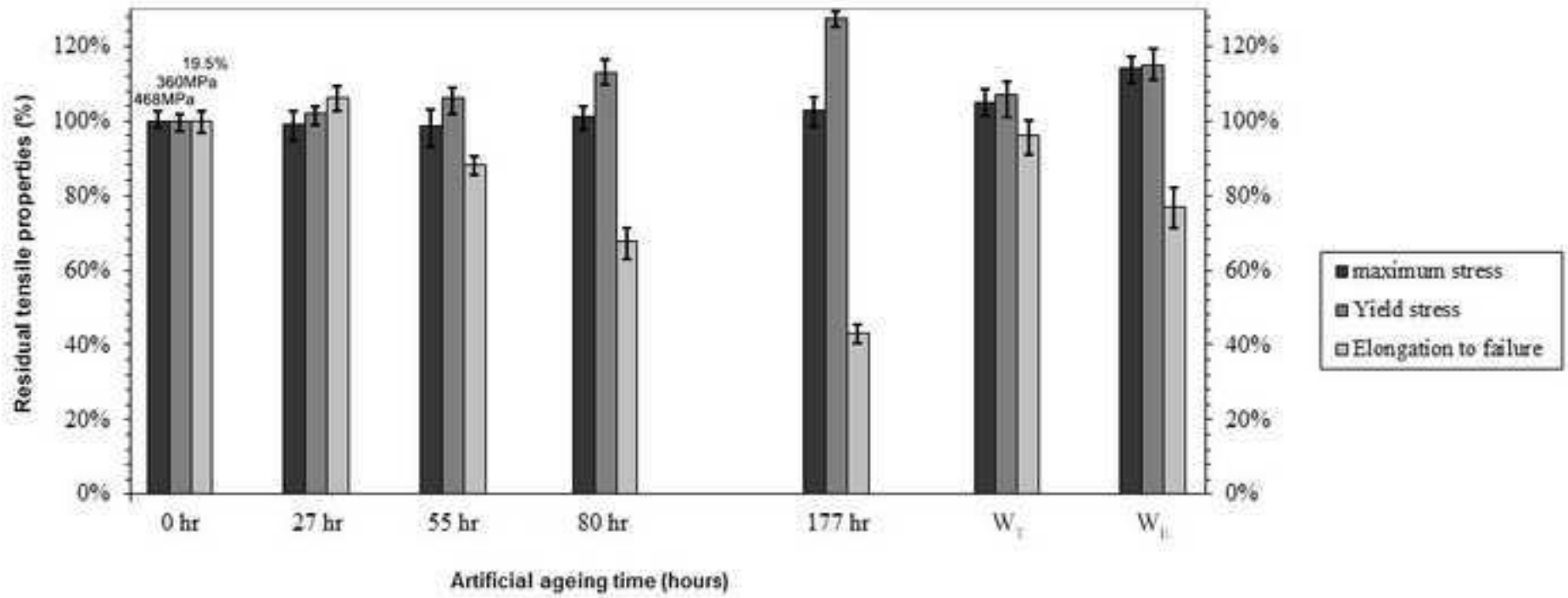
19.5%
360MPa
468MPa
120%
100%
80%
60%
40%
20%
0%
Residual tensile properties (%)
0 hr
27 hr
55 hr
80 hr
177 hr
W
W
Artificial ageing time (hours)
maximum stress
Yield stress
Elongation to failure

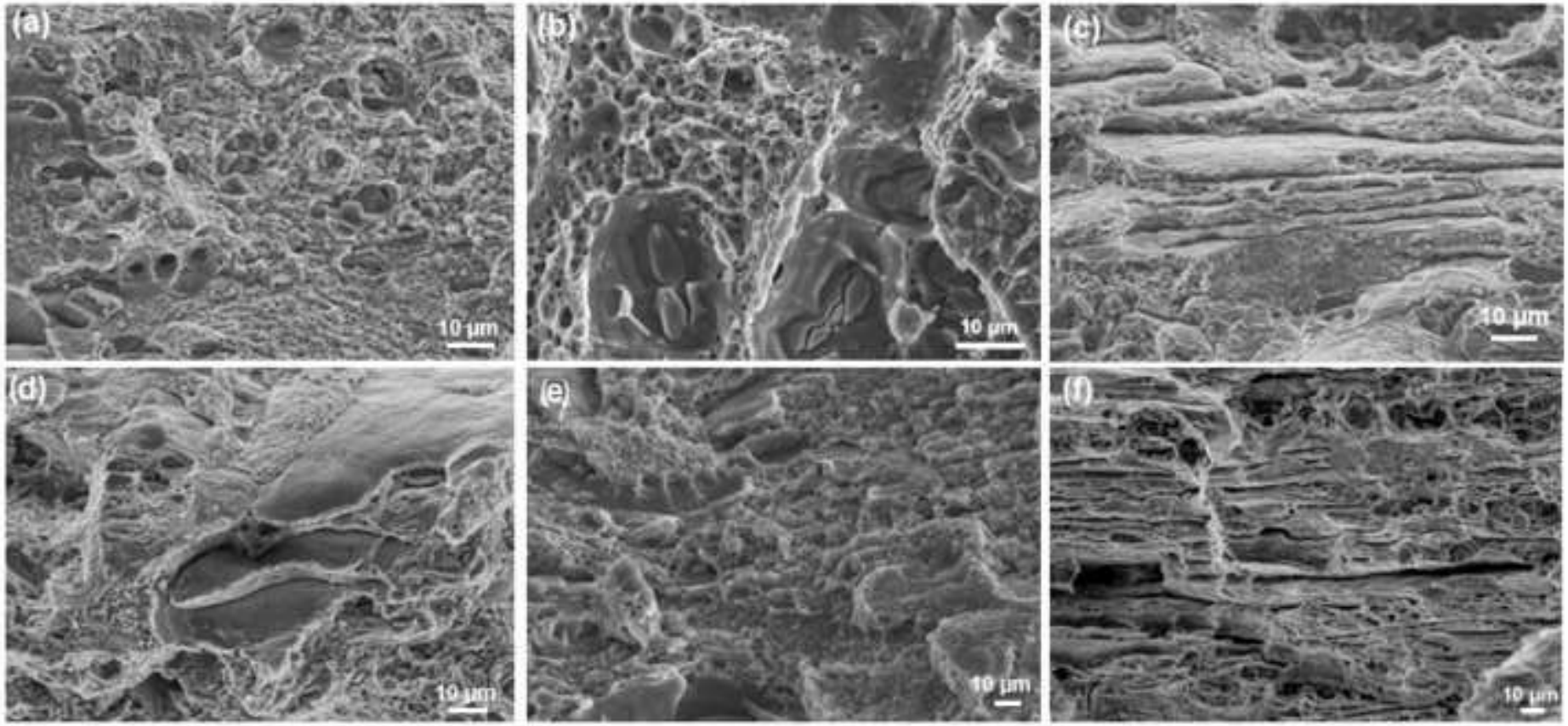
(a)
10 μm
(b)
10 μm
(c)
10 μm
(d)
10 μm
(e)
10 μm
(f)
10 μm

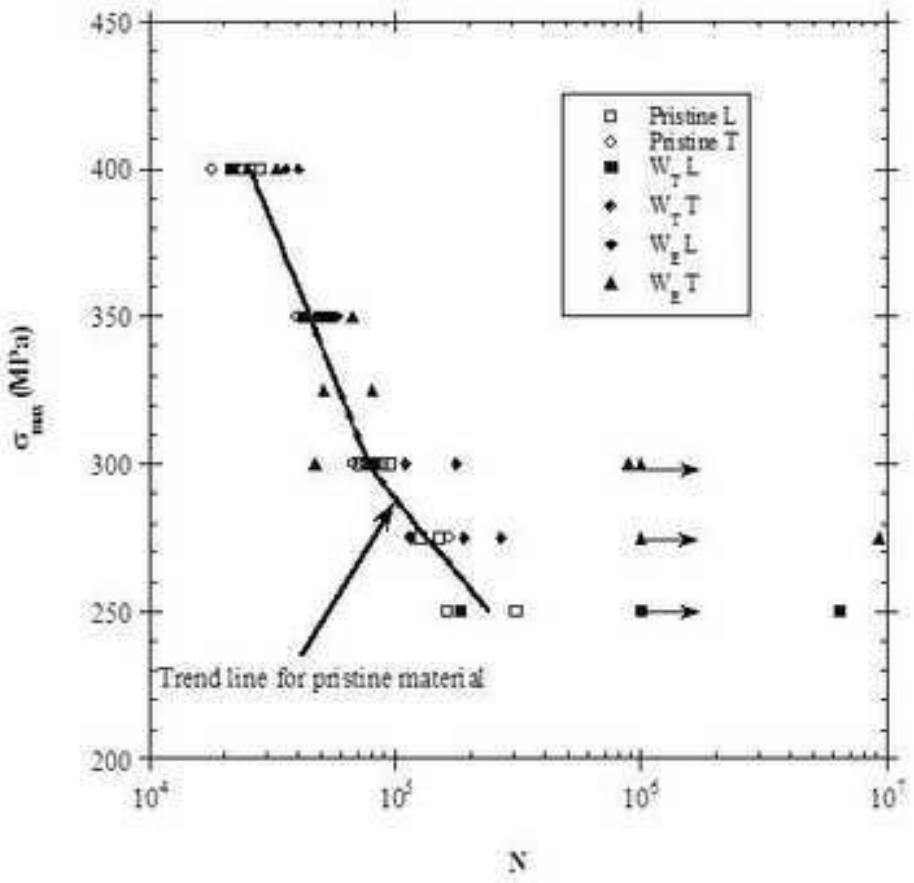
450
400
350
300
250
200
10^4
10^5
10^6
10^7
σ_{max} (MPa)
N
Pristine L
Pristine T
W_T L
W_T T
W_E L
W_E T
Trend line for pristine material

(a)

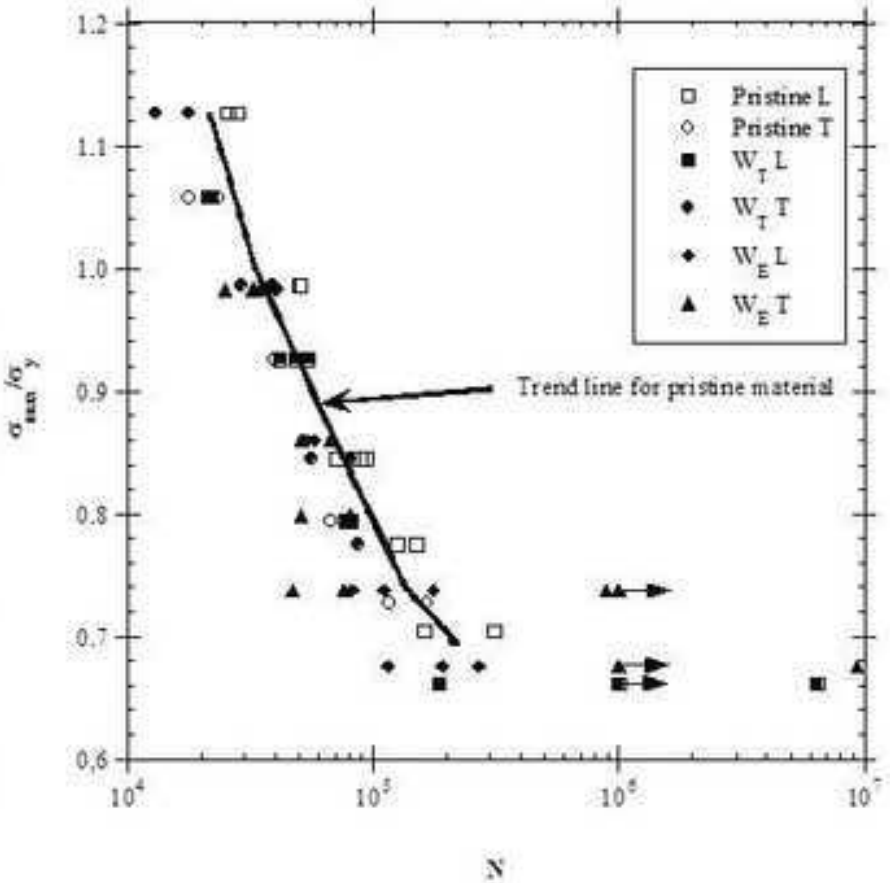
1.2
1.1
1.0
0.9
0.8
0.7
0,6
10^4
10^5
10^6
10^7
σ_{max}/σ_y
N
Pristine L
Pristine T
W_T L
W_T T
W_E L
W_E T
Trend line for pristine material

(b)

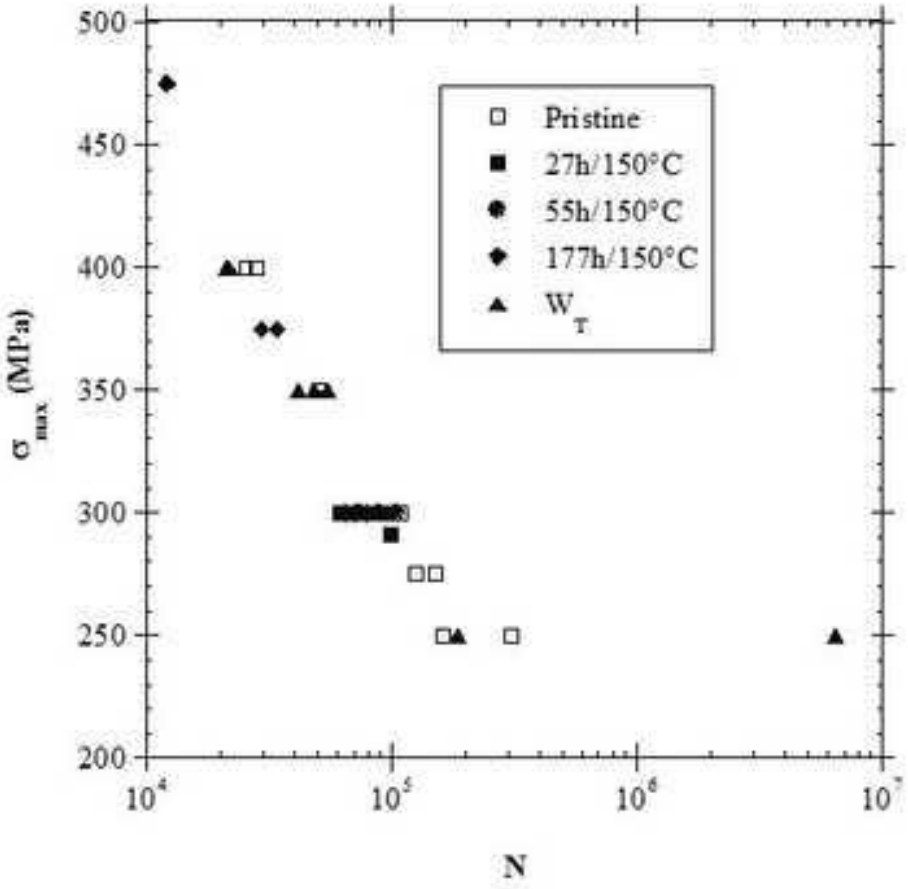
500
450
400
350
300
250
200
σ_{max} (MPa)
10^4
10^5
10^6
10^7
N
Pristine
27h/150°C
55h/150°C
177h/150°C
W_T

(a)

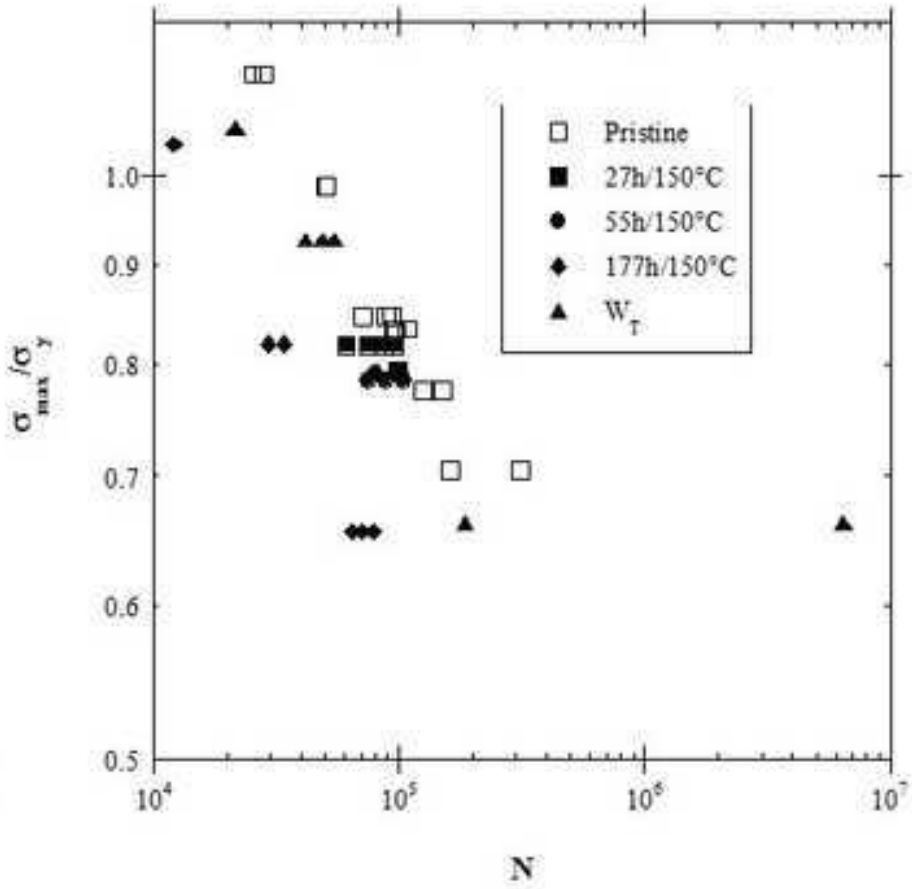
1.0
0.9
0.8
0.7
0.6
0.5
σ_{max}/σ_y
10^4
10^5
10^6
10^7
N
Pristine
27h/150°C
55h/150°C
177h/150°C
W_T

(b)

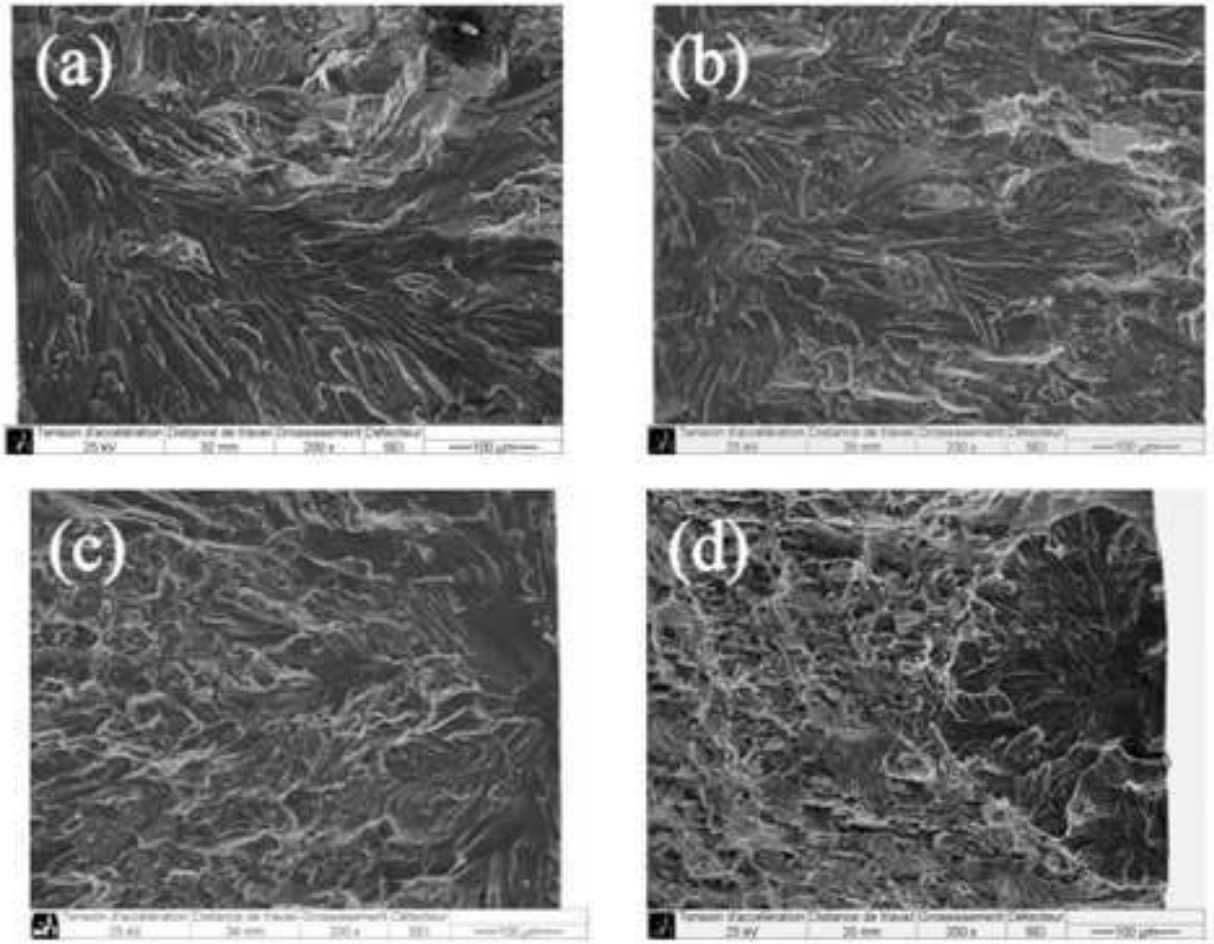
(a)
(b)
(c)
(d)

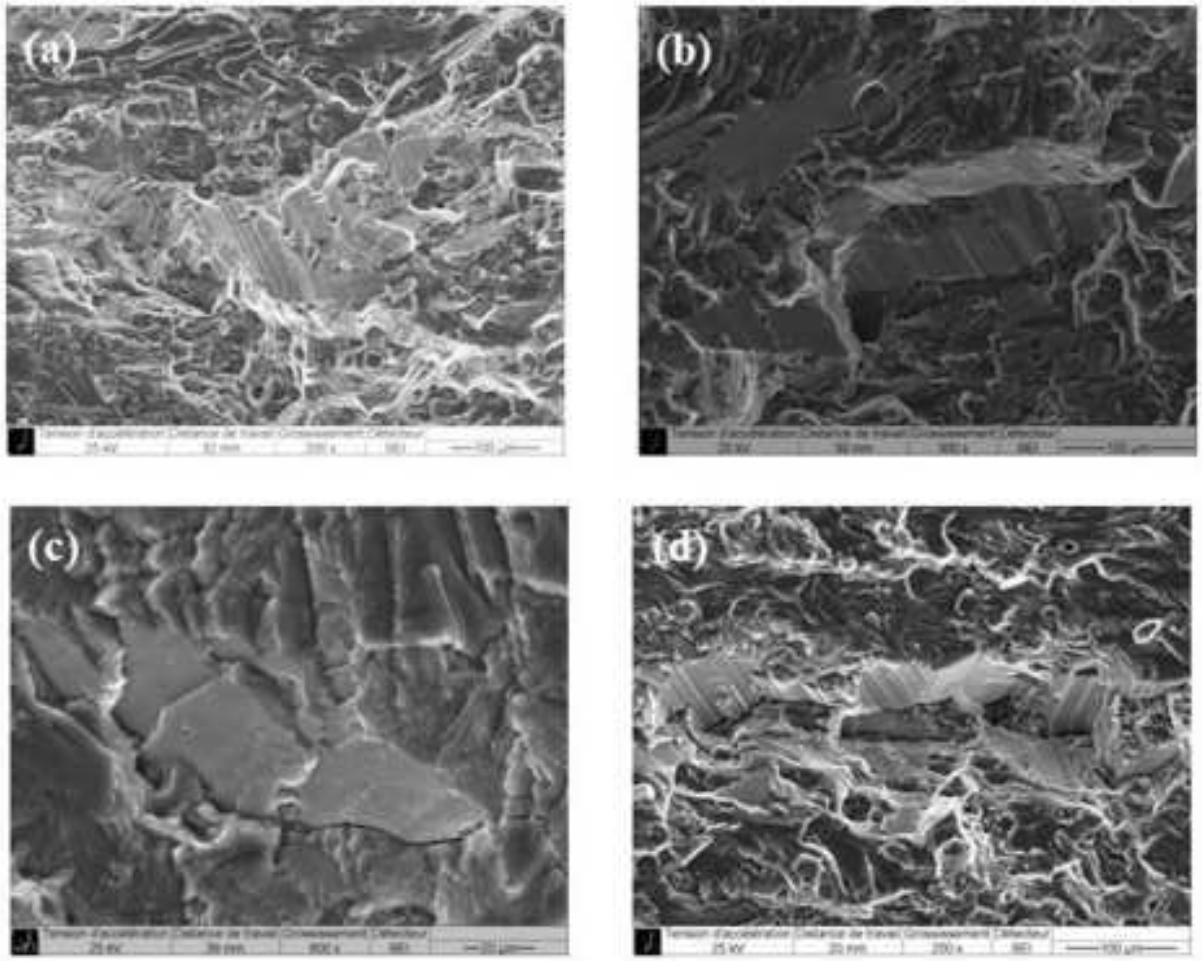
(a)
(b)
(c)
(d)

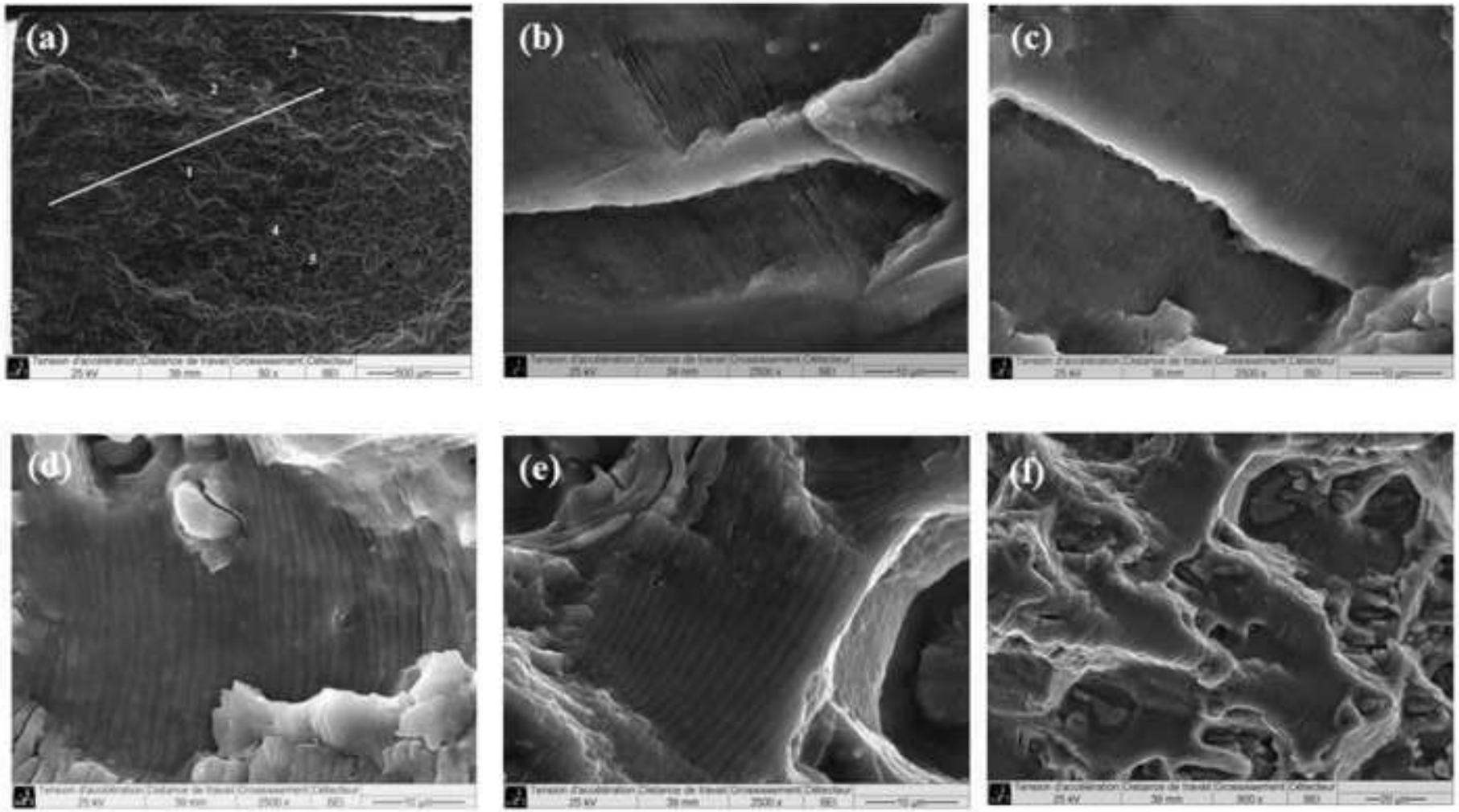
(a)
1
2
3
4
5
(b)
(c)
(d)
(e)
(f)

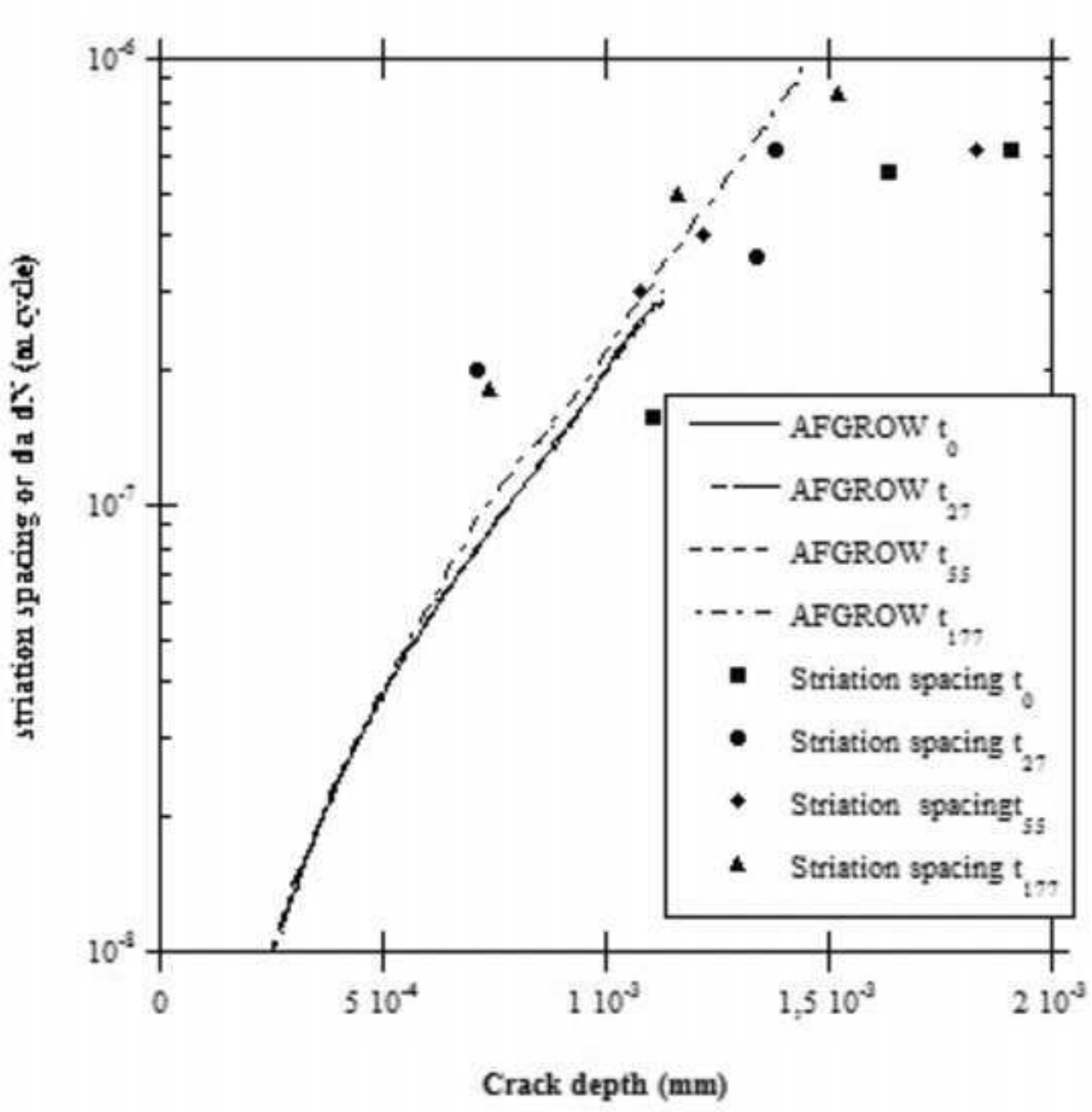
striation spacing or da dN (m cycle)
10⁻⁶
10⁻⁷
10⁻⁸
0
5 10⁻⁴
1 10⁻³
1,5 10⁻³
2 10⁻³
Crack depth (mm)
AFGROW t0
AFGROW t27
AFGROW t55
AFGROW t177
Striation spacing t0
Striation spacing t27
Striation spacingt55
Striation spacing t177

- The mechanical performances of AA 2024 from the teardown of a decommissioned A320 aircraft are compared to those of an artificially aged material
- Microstructural modifications induced by ageing are studied by light and electronic microscopy and by electrical conductivity measurements
- The results are similar for the material at the end of the service life and for a material aged for 55h at 150°C
- More significant modifications can be anticipated for longer exposures (177h at 150°C)

Artificial aging at 150°C	**Aircraft aging at 80°C**
t_0	0 h
t_{27}	50 000 h
t_{55}	100 000 h
t_{80}	145 000 h
t_{177}	319 676 h

	Al	Cu	Mg	Mn	Fe	Si	Ti
Pristine material	balance	4.46	1.44	0.61	0.13	0.06	0.03
Wing panels	balance	3.98	1.32	0.66	0.07	0.07	0.02

	Initial Flaw Size (computed)		Initial Flaw Size (experimental)			
Aging condition	c_0 (µm) computed	a_0 (µm) computed	c_0 (µm) experimental	a_0 (µm) experimental	N_f computed	N_f experimental
t_0	85	52	113	33	95 581	95 006
t_{27}	88	81	89	77	75 157	74 663
t_{55}	62	62	62	62	105 034	104 602
t_{177}	85	97	82	103	64 030	64 486
W_E	58,8	58,8	78	78	82 019	81 973

a